# Investigation of the Internal functioning of the Radial Basis function neural network river flow forecasting models

D. Achela K. Fernando[1] and Asaad Y. Shamseldin[2]

## Abstract

This paper deals with the challenging problem of hydrological interpretation of the internal functioning of ANNs by extracting knowledge from their solutions. The neural network used in this study is based on the structure of the Radial Basis Function Neural Network (RBFNN) which is considered as an alternative to the Multi Layer Perceptron (MLPNN) for solving complex modelling problems. This network consists of an input, hidden and an output layer. The network is trained using the daily data of two catchments having different characteristics and from two different regions in the world. The present day and antecedent observed discharges are used as inputs to the network to forecast the flow one day ahead. A range of quantitative and qualitative techniques are used for hydrological interpretation of the internal functioning by examining the responses of the hidden layer neurons. The results of the study show that a single hidden layered RBFNN is an effective tool to forecast the daily flows and that the activation of the hidden layer nodes are far from arbitrary but appear to represent flow components of the predicted hydrograph. The results of the study confirm that the three neurons in the hidden layer of this model effectively divide the input data space in such a way that the contribution from each neurone dominates in one of the flow domains – low, medium or high – and form, in a crude manner, the base flow, interflow and surface runoff components of the hydrograph.

Keywords (Artificial Neural Networks, Radial Basis Function, hidden neurons, hydrological interpretation)

[1] Lecturer, School of the Built Environment, Unitec New Zealand, Private Bag 92025, Auckland, New Zealand

[2] Senior Lecturer, Department of Civil and Environmental Engineering, The University of Auckland, Private Bag 92019, Auckland, New Zealand

## Introduction

While various soft modelling approaches are used in flow forecasting (Chau 2006; Chau et al. 2005), artificial neural networks (ANNs) have emerged as one of the very popular hydrological modelling tool. It has been applied to diverse hydrological modelling problems such as rainfall-runoff modelling, river flow forecasting, flood estimation and groundwater (Coppola et al. 2003 ; Dawson et al. 2006; Wu et al. 2005). What has emerged from these applications is that ANNs can produce results which are at least comparable or better than those obtained using traditional hydrological models. However, despite these promising results, there is still a need for advanced research on ANNs to realise their full potential in hydrological modelling (De Vos and Rientjes 2005).

ANNs are basically data-driven input-output models which are dependent on the observed hydrological data to extract the corresponding input-output relations. ANNs have many powerful characteristics which have contributed to their success and popularity in the field of hydrological modelling. They are very powerful in modelling complex non-linear relationships with little prior knowledge and they can be quickly and easily developed.

However, they have a number of disadvantages which have led to some criticisms and reluctance to accept their use in the field of hydrology (De Vos and Rientjes 2005; Gaume and Gosset 2003; Jain et al. 2004). Firstly, they do not explicitly account for physical processes taking little or no use of the prior available hydrological knowledge. Secondly, the modelling solutions provided by ANNs are opaque in the sense that little is known about the type of hydrological knowledge being extracted from the solutions. Most of the studies concerned with the hydrological application of ANNs do not examine

the internal behaviour of ANN from a hydrological point of view which can hold the key to revealing the hydrological knowledge being extracted by the ANN modelling solutions. The lack of this examination may to some extent be due to the structure of the ANN commercial software packages which do not allow the user to extract information relevant to the internal functioning of ANNs.

Attempts have been made in the past to interpret the meaning of ANN model parameters and to extract rules for the operation of ANNs (Garson 1991; Rabuñal et al. 2004). The hydrological interpretation of the internal functioning of ANN has become a major challenge to the ANN enthusiasts modelling hydro-meteorological phenomena. Only in the most recent years have a few publications emerged attempting to explain the internal functioning of the ANNs and extract relevant knowledge (Jain et al. 2004; Lozowski et al. 1996; Tickle et al. 1998; Wilby et al. 2003). Most of these publications have focused mainly on explanation of the multi-layer perceptron neural network (MLPNN) which is the most widely used in hydrological modelling as well as in other fields. However, there are other types of ANNs which may have similar capabilities in extracting hydrological knowledge.

In some of the hydrological publications dealing with knowledge extractions from the ANN solutions, the investigations have been carried out using observed data and synthetic "error-free" data generated from other traditional hydrological models. Dibike et al. (Dibike et al. 1999) trained an ANN to simulate the synthetic water level data generated by a hydraulic model. They found that the ANN can successfully encapsulate the hydraulic knowledge and site-specific data. Wilby et al. (2003) used synthetic "error-free" discharge time series generated for a quasi-physical conceptual rainfall-runoff model to investigate the internal behaviour of the standard MLPNN. The MLPNN

consisted of input, hidden and output layers and used the daily rainfall and the evaporation data as input information to provide estimates of the synthetic discharge time series. Their results showed that the neurons of the hidden layer were able to capture the dominant processes simulated by the quasi-physical model, namely, the *quick-flow* and the *base-flow* components. Likewise, Jain et al. (2004) trained the standard MLPNN using the synthetic discharge generated from a quasi-physical conceptual rainfall model as an external network output. The present and previous rainfall values as well as past observed discharges were used as the external inputs to the network. The results of their work demonstrated that the hidden neurons were able to approximate various hydrological physical processes such as infiltration, base flow and quick flow.

The internal functioning of the ANNs has also been investigated using actual observed data. For example, Sudheer and Jain (Sudheer and Jain 2003) developed a visualization framework for examining the internal behaviour of the MLPNN. This framework is based on the development of a rank curve/flow duration curve of the observed flow data and plotting the corresponding hidden neuron responses on the graph as the rank curve of the observed flow data. The framework was applied to the results obtained from a non-linear autoregressive MLPNN river flow forecasting model. They found that the neurons of the hidden layer partitioned the domain of the transfer function used in conjunction with the hidden neurons into sub-regions with the final network output being a weighted sum of the responses from these sub-regions. and that the external inputs influence the shape of the estimated hydrograph in different ways. Similarly, Shamseldin et al. (Shamseldin et al. 2005) investigated the contribution of the hidden neurons to the final network output of a non-linear autoregressive MLPNN river flow forecasting model using the data of two catchments. The hidden layer of standard

MLPNN used in their study consisted of three hidden neurons. The results of the above study confirmed the existence of *dominance effects* with one of the hidden neurons doing most of the work while the other two provided a complex non-linear correction to the high and low flow magnitudes.

In similar vein to the above encouraging studies dealing with investigation of internal functioning of ANNs, this paper for the first time will provide insight into the internal functioning of a neural network type known as the Radial Basis Function (RBF) neural network (RBFNN). The RBFNN was originally proposed as an alternative to the MLPNN for solving complex modelling problems (Luo and Unbehauen 1999). In principle, the configuration of the RBFNN is quite similar to that of the MLPNN. However, there are differences between the RBFNN and the MLPNN regarding the mathematical operations involved in the input-output transformation. The principal aim of this paper is to test whether hydrological knowledge can be extracted from neural networks other than the MLPANN, the most popular one.

The RBFNN used in this study is basically a non-linear auto-regressive model using the current and previous observed daily flow as inputs in order to estimate the one-day-ahead flow forecast. The investigation of the internal functioning of the RBFNN is carried out using the daily discharge data of two catchments, namely, the Blue Nile and the Brosna catchments; the former is located in Africa while the latter is located in Ireland.

The present paper is structured as follows. The next section explains the general structure of the RBFNN and the procedure used for its calibration. It is followed by a brief description of the catchments used in the study. The section thereafter is devoted to

discussing the results of the study. The main conclusions of the paper and the limitations of this study are given in the last section.

**Description of the Radial Basis Function (RBF) Neural Network**

The RBFNN used in this study is a three layered feed-forward network with the hidden layer composed of three nodes performing a transformation according to an RBF. The number of hidden nodes is usually unknown *a-priori*. The RBFNNs are normally considered as universal approximators (Hartman et al. 1990; Park and Sandberg 1991; Park and Sandberg 1993) which can approximate any function to an arbitrary accuracy, provided that the size of network is not constrained. Applications of RBFNN are widespread and can be found in function approximation problems (Leonard et al. 1992), prediction of time series (Shepherd and Broomhead 1990), system modelling (Chen et al. 1990), and hydrological modelling (Dawson et al. 2006; Jayawardena and Fernando 1998). General description of the RBFNNs can be found in many of the standard ANN text books (e.g. Haykin, 1999) and their specific mathematical representations as applied to flow forecasting are also available (Fernando and Jayawardena 1998). A brief description of the RBFNN used in this study is given below.

The RBFNN has an input, a hidden, and an output layer of nodes. Figure 1 shows a schematic diagram of the RBFNN used in this study with 3, 3 and 1 nodes in the input, hidden and output layers, respectively.

The 3-dimensional input patterns of antecedent flow rates (**X)** are being mapped to 1-dimensional output, the daily flow forecast (**Z)**. The nodes in the adjacent layers are exhaustively connected. The number of nodes in the hidden layer is problem dependent, and in this study, there are three whose role in the representation of the mapping from **X**

to **Z** is investigated. Although, this number can be optimized, this is not done here as the main focus of the study is on knowledge extraction rather than estimating the optimum number of hidden nodes. In a separate study, a sensitivity test revealed that prior knowledge of the catchment with regard to the nature of the flow can be made to assist in determining an optimum number of hidden layer nodes (Fernando and Shamseldin 2007).

The transfer functions *f* in the hidden layer nodes are RBFs or *kernel* functions. These RBFs are defined by their centres ($\mathbf{U}_1$, $\mathbf{U}_2$, $\mathbf{U}_3$), where the function activation is highest, and the spread ($\boldsymbol{\sigma}_1$, $\boldsymbol{\sigma}_2$, $\boldsymbol{\sigma}_3$) which define the extent of the receptive field.

When the input pattern for the $p^{th}$ time step, made up of three antecedent flow daily values, $x_{p1}$, $x_{p2}$, $x_{p3}$, is $\mathbf{X^P}$=[ $x_{p1}$ $x_{p2}$ $x_{p3}$] and the RBF centres are $U_1 = [u_{11},u_{12},u_{13}]$, $U_2 = [u_{21},u_{22},u_{23}]$ and $U_3 = [u_{31},u_{32},u_{33}]$, then, the response of the $j^{th}$ hidden neurone $h_{pj}$ due to $p^{th}$ input pattern $\mathbf{X}^P$ is given by

$$\begin{bmatrix} h_{P1} \\ h_{P2} \\ h_{P3} \end{bmatrix} = \begin{bmatrix} \exp\{-(\frac{[x_{P1}-u_{11}]^2}{2\sigma_1^2}+\frac{[x_{P2}-u_{12}]^2}{2\sigma_1^2}+\frac{[x_{P3}-u_{13}]^2}{2\sigma_1^2})\} \\ \exp\{-(\frac{[x_{P1}-u_{21}]^2}{2\sigma_2^2}+\frac{[x_{P2}-u_{22}]^2}{2\sigma_2^2})+\frac{[x_{P3}-u_{23}]^2}{2\sigma_2^2}\} \\ \exp\{-(\frac{[x_{P1}-u_{31}]^2}{2\sigma_3^2}+\frac{[x_{P2}-u_{32}]^2}{2\sigma_3^2}+\frac{[x_{P3}-u_{33}]^2}{2\sigma_3^2})\} \end{bmatrix} \quad \ldots\ldots\ldots\ldots\ldots\ldots\ldots\ldots(1)$$

The output from each hidden node is $Out_{pj}$ (j=1,2,3) is made up of the product of hidden response and the weight of the output layer synaptic connection $w_{j1}$ (j=1,2,3), i.e.,

$Out_{pj} = h_{pj} \times w_{j1}$ ; j=1,2,3 ……(2)

Accordingly, the RBFNN output for the $p^{th}$ pattern is given by

$$z_P = Out_{p1} + Out_{p2} + Out_{p3} = h_{P1}w_{11} + h_{P2}w_{21} + h_{P3}w_{31} \quad \ldots\ldots\ldots\ldots\ldots\ldots\ldots\ldots(3)$$

In the case of single output, this can be further simplified to

$$z_P = Out_{p1} + Out_{p2} + Out_{p3} = h_{P1}w_1 + h_{P2}w_2 + h_{P3}w_3 \quad \text{.....(4)}$$

The proportional contribution from the hidden nodes $PC_{pj}$ to the output $Z_p$ can be calculated according to the following equation:

$$PC_{pj} = \frac{out_{pj}}{Z_p} \quad \text{.....(5)}$$

In this study, in order to understand the internal functionality of the RBFNN, the examination of the hidden node responses ($h_{pj}$) involves the calculations of the individual contributions from the hidden nodes ($out_{pj}$) and the proportional contributions from the hidden nodes ($PC_{pj}$).

The parameters of the RBF function (i.e. the centre $\mathbf{U}_j$ and spread $\boldsymbol{\sigma}_j$) together with the output layer weights $w_1$, $w_2$, and $w_3$, constitute the RBF model parameters. Accordingly, the calibration of the RBFFN model entails determining the optimum parameters for the three hidden nodes and the three output layer weights.

Optimum parameters of an RBFFN can be determined by many methods of varying complexity, some of which are non-iterative clustering (Specht 1991), k-means clustering (Jayawardena and Fernando 1998), orthogonal least squares (Chen and Billings 1989; Fernando and Jayawardena 1998). In this study, the conjugate gradient-descent algorithm is used to minimise the sum of the squares of errors between the observed and forecasted flows in order to determine the RBF centres, their spreads, and the connection weights between the hidden and the output layer.

The RBF centres are essentially vectors representing points in the input space, which in this study is 3-D. Given that the input data space can only span from the minimum to the maximum flow values obtained from the calibration period, the RBF centres can logically be constrained to the 3-dimensional space dictated by the range of

the daily antecedent flows. Hence, the following constraints were imposed on these parameters during the calibration of the RBFNN:

$$u_{ij} \le Q_{max} \;;\; u_{ij} \ge Q_{min} \;;\; u_{ij} \ge 0 \text{ and } \sigma_j \le Q_{max} \;;\; \sigma_j \ge Q_{min} \;;\; \sigma_j \ge 0 \quad \text{....(6)}$$

where i = 1, 2, 3; j = 1, 2, 3; and $Q_{max}$ and $Q_{min}$ refer to the maximum and minimum flow values in the training data set, respectively. Although, the visualisation of the input space when dealing with three dimensional input is practical (See Fig 2a & 2b), it is somewhat difficult for input patterns of higher dimensions. However, the concept of constraining the centres to lie within the periphery of the input space holds appropriate regardless of the dimensionality of the input space.

**Catchments**

The River Brosna is located in Ireland. This river flows through one of the largest areas of bog land which is regarded as a significant factor that influences its catchment response to rainfall events. This river has experienced very extensive remedial schemes to improve drainage. The catchment has flat topography and temperate climate. The rainfall occurs in this catchment throughout the year with the maximum rainfall occurring during the winter months. The catchment area is 1207km$^2$ receiving, on average, 800 mm of rainfall with a mean daily discharge of 14m$^3$/s.

The Blue Nile and its tributaries arise on the Ethiopian Plateau originating from a small spring to the south of Lake Tana (Sutcliffe and Parks, 1999). It then flows through the lake down through Ethiopia and Sudan, to meet the White Nile at Khartoum (capital of Sudan) which marks the start of the great River Nile. The Blue Nile is one of the main

tributaries to the River Nile, contributing about 60% of annual flow. The catchment area upstream El Deim station used in this study is 254,230km$^2$ with the average annual rainfall in the basin varying between 1000mm near the Sudanese-Ethiopian border to 1800mm in the uppermost sections. The rainfall is seasonal with intense rainfall occurring during the summer season. The rainfall in this catchment is highly influenced by the movement of the Inter-Tropical Convergence Zone [ITCZ] controlling the seasonal rainfall pattern (Sutcliffe and Parks 1999). About 80% of the annual discharge occurring in a flood season that runs from June to October causes a sharp seasonal peak in annual discharge to occur in late August or September. The mean daily flow of this river is around 1550 m$^3$/s.

**Analysis**

The daily discharge data spanning eight years for the two rivers were separated into training/calibration and testing/verification sets as summarised in Table 1. Although various proportions of the data sets could have been used to make up the training and testing sets, a 50% split was used for simplicity. Also, it was noted that when the data sets were divided into equal parts, the former half included the full range of flow values in the entire data set making it a good representative set to be used as the traning/calibration set.

Preliminary examination of the autocorrelation of the daily flow data for the two stations, as shown in the Figure 3, revealed that the correlation is significant (autocorrelation coefficient > 0.8) up to three units of lag time (3 days) for Brosna indicating that the three antecedent flow values have the greatest influence on the subsequent value of discharge. As expected, for Blue Nile too the correlation gradually decreases with increasing lag time. In order to compare similar networks on different

catchments, the most recent three antecedent flow values were selected as inputs to the network for both cases. Thus, the purpose of the model was to make one-day-ahead flow forecasts for the two stations using the flow values in the three antecedent days.

The optimum values of the RBF centres and spreads for the three hidden layer nodes in each of the RBFNN model were found using the conjugate gradient descent technique minimising the sum of the squares of the errors between the forecast flows and observed flows for the training data set subject to the constraints given by equation (6).

Figures 2a, 2b and 4a 4b, demonstrate the distribution of the input data and the three selected RBF centres in the input space. Table 2 summarises the key features of the input data and the optimum network parameters obtained during training.

Having calibrated the RBFNN, the hidden layer node response ($H_{pj}$), the contribution from each hidden node to the output ($Out_{pj}$), and the proportion of contribution from each hidden node towards the forecast flow ($PC_{pj}$) were calculated to investigate the internal operation of the RBFNN.

***The Blue Nile Catchment***

Figure 5 plots the hidden node responses (Hpi) on the primary y-axis and the comparison between actual (Q) and flow forecast (Z) flow on the secondary y-axis. The flow forecasts, as seen in Figure 5 has a high correlation to the observed flows as confirmed by the high correlation coefficient of 96.91%.

Figures 6a gives a more close-up view of a period of one year where the hidden node responses can be more clearly evaluated while Figure 6b illustrates the proportional contribution from the hidden nodes $PC_{pj}$ to the output for the same duration. These figures provide an insight into the stages of the hydrograph at which each hidden neuron activates and the relative magnitudes of their contribution to the final network output.

Figure 7 shows the actual contribution from the hidden nodes $Out_{pj}$ towards the network output in a stacked up format to demonstrate that not only do the contributions from the hidden nodes cumulatively account for the forecast flows, but also that each contribution appears to represent a flow component. For example, the flow component $outp_1$ resembles the base flow component which can be extracted using the variable slope method. It could be thought that the three neurons crudely correspond to the usual flow components, namely, baseflow, interflow and surface runoff, respectively. Each neurone appear to represent a "local model" responsible for generating runoff in the low, medium and high flow ranges. The RBF centres in the scatter plots in Figure 2 for the Blue Nile river are located at low, medium and high regions of the input space. This intrinsic property of the RBF network that divides the input space is a contributing factor in the reconstruction of the flow from its components.

Examination of Figures 6a and 6b reveal a very complex interaction between the operations of the three hidden neurons. According to Figure 6a, the response from each hidden node is significant only at specific ranges of flow values. For example, $H_{p1}$ output is significant only during low flow period. Likewise, the output $H_{p2}$ becomes significant in the medium/high flows and the output $H_{p3}$ becomes significant in the high flow region. Coupled with the weights of the connections, each of these hidden nodes makes a partial contribution to the forecast flow; the relative contribution varies with the flow magnitude. Figure 6b shows that in fact, the operation of these neurons is dependent on two flow magnitudes, namely, ~0.8 mm/day and ~1.8 mm/day. As such, this river flow domain can be divided into three distinct flow zones, namely, low, medium/high and very high.

It is also evident from the figure that $H_{p1}$ and $H_{p2}$ respond more quickly than $H_{p3}$ to changes in the discharge hydrograph. At the threshold of ~0.8mm/day the proportional contribution of hidden neuron 1 ($PC_{p1}$) is at its maximum value, after which it starts to decrease until it becomes insignificant at very high flows. Likewise, the proportional contribution $PC_{p2}$ is the minimum at the 0.8mm/day flow magnitude reaching a maximum value at a flow magnitude of 1.8 mm/day beyond which its contribution decreases for very high flow values greater than 2mm/day. Node 3, on the other hand, remains relatively dormant and begins to be an active contributor as the flow reaches medium/high values. Its contribution steadily increases from a minimum value of 1mm/day until it dominates the network operation at very high flow values.

Inspection of figure 7, confirms the existence of "dominant effects" and "local models" where the hidden nodes take turns in the overall operation of the RBF either individually or collectively. The low flow range (<0.5mm/day) is dominated by $Out_{p1}$ and $Out_{p2}$ contributing around 80% of the network output, with Node 1 being the more dominant neuron. In the medium/high flow range (0.5 – 1mm/day) the Node 2 gradually takes over the dominance from Node 1 in the rising limb of the hydrograph and hands back the dominance to Node 1 in the falling limb. In the very high flow zone, Nodes 2 and 3 dominate the operation of the network. This behaviour of the hidden neurones can be perceived as being local models that mimic the performance of soil storage reservoirs that generate flow components resembling baseflow, interflow and quick runoff components although there was no such prior knowledge explicitly included into the RBFNN model development. This illustrates that the RBFNN model is able to systematically decompose the flow hydrograph into some meaningful flow components in this catchment.

The interesting observation of the mutual dominance of Nodes 1 and 2 in the rising and falling limb of the hydrograph suggests that it may be representative of the natural scenario where the interflow becomes dominant leading to the wet season and the base flow gradually taking over during the recession leading to dry season.

***Brosna River***

The average flow rate in this river is comparatively low with significant fluctuations. The RBF centres for Brosna river flow data are spatially distributed as shown in Figure 4. As seen in Figure 8, the correlation coefficient ($R^2$ = 88.48%) for one-day ahead forecasts indicates that this RBFNN is fairly effective in forecasting daily flows. However, it must be noted that the model does not perform very well in the high flow range encountered in the fourth year of the training data set. This trend is continued in the testing set of four years that follow.

Figure 9a shows the response of each hidden neuron where Node 2 is largely responsive during what appears to be the dry-weather flow, and that the two remaining nodes show significant activation during the wetter season. As seen in Figure 9b, the proportional contribution of the hidden nodes towards the network output is dependent on

a flow magnitude threshold of 0.7 mm/day. In the low flow region where the flow magnitude is less than 0.7 mm/day Node 2 dominates the operation of the RBFNN contributing around 70% of the RBFNN river flow forecasts. As the flow reaches the medium high zone, the Node 2 gradually looses its dominance handing it to the other two neurons until its contribution to the final RBFNN output is non-existent. In the peak flow range in excess of ~1.5 mm/day, the local models from Nodes 1 and 3 completely account for the network output.

The figures also show that there is a close association between the operation of Nodes 1 and 3 both of which mirror with some delay the variation patterns in the discharge hydrograph. However, Node 2 mirrors the changes in the discharge hydrograph in a reverse manner. From these observations and from Figure 10, it can be seen that similar to the Blue Nile, this behaviour of the hidden neurones can be perceived as mimicking the action of local models that generate flow components belonging to specific flow ranges. The components crudely represent baseflow, interflow and quick runoff components although it is not as pronounced as in the Blue Nile case.

**Discussion and conclusions**

The above analysis reveals that the RBFNN, although generally regarded as a black-box type of model, has its hidden neurons performing specific roles in the process of forecasting river flow. The hidden neurons clearly have designated roles to play in their respective flow domains, each resembling a local model that generates a flow component. As can be expected from RBFs, the influence or the activation of a given neuron is dictated by the location of the centre and limited by the spread of the basis function. The RBF centres for the Blue Nile river flow forecasting model is such that they span the entire input space with a clear separation between their effective domains (Fig 2b). In the case of the Brosna river on the other hand, there may be overlap of these domains (Fig 2b and Table 1). As the activity of a hidden neuron is prompted by the division of the flow domain in the training data, the knowledge of the catchment and flow characteristics may be made use of in determining the number of discernible flow components (base flow and fast run off only, or base, interflow and quick runoff) and thereby the number of hidden neurones. Further investigation with different types of catchments and flow

characteristics is required to understand the sensitivity of the number of RBFs to adequately represent the physical processes.

The following conclusions can be made:

(1) The RBFNN can be trained to develop an effective daily flow forecasting tool for two rivers with different flow characteristics.

(2) The activation of the hidden nodes in the RBFNN is not arbitrary and can be related to flow components in the hydrograph that crudely represent the hydrological processes in the catchment. The three hidden neurons used in this study activate and, through the weights in the output layer, contribute to the forecast flow value in a manner that is perceived to be mimicking local models that generate flow components in the three flow domains – low, medium and high.

(3) The proportional contribution from each hidden neurone varies over the forecast period reflecting the dominance of the local models in a given region of the flow domain.

(4) The RBFNN with its parameters (RBF centres and spreads and the output layer connection weights) seem to function in such a way that the contributions from the hidden neurons represent flow components that resembles the baseflow, interflow and runoff components of the flow hydrograph particularly in the case of Blue Nile river. It may be possible to use the knowledge of the specific runoff characteristics of catchments to predetermine the optimum RBFs in the forecast model.

The results obtained in this paper using a limited number of catchments indicate that the operation of the RBFNN is not entirely arbitrary but generate meaningful flow components specific to the catchment. Consideration should be given, in the future studies, to apply the methodology to a large number of catchments using different RBFNN structures and external inputs to investigate the sensitivity of the network structure.

**References**

Chau, K. W. (2006). "Particle swarm optimization training algorithm for ANNs in stage prediction of Shing Mun River." *Journal of Hydrology*, 329(3-4), 363-367.

Chau, K. W., Wu, C. L., and Li, Y. S. (2005). "Comparison of several flood forecasting models in Yangtze River." *Journal of Hydrologic Engineering, ASCE*, 10(6), 485-491.

Chen, S., and Billings, S. A. (1989). "Extended model set, global data and threshold model identification of several non-linear systems." *International Journal of Controls*, 50(5), 1897-1923.

Chen, S., Billings, S. A., Cowen, C. F. N., and Grant, P. M. (1990). "Non-linear systems identification using radial basis functions." *International Journal of Systems Science*, 21(12), 77-93.

Coppola, J. E., Poulton, M., Charles, E., Dustman, J., and Szidarovszky, F. (2003 ). "Application of Artificial Neural Networks to Complex Groundwater Management Problems." *Natural Resources Research*, 12(4), 303-320.

Dawson, C. W., Abrahart, R. J., Shamseldin, A. Y., and Wilby, R. L. (2006). "Flood estimation at ungauged sites using artificial neural networks." *Journal of Hydrology* 319(1-4), 391-409.

De Vos, N. J., and Rientjes, T. H. M. (2005). "Constraints of artificial neural networks for rainfall-runoff modelling: trade-offs in hydrological state representation and model evaluation." *Hydrology and Earth System Sciences*, 9, 111-126.

Dibike, Y. B., Solomatine, D. P., and Abbott, M. B. (1999). "On the encapsulation of numerical-hydraulic models in artificial neural network." *Journal of Hydraulic Research*, 37(2), 147-161.

Fernando, A. K., and Shamseldin, A. Y. "Role of hidden neurons in a RBF type ANN in stream flow forecasting." *MODSIM 2007 - International Congress on Modelling and Simulation*, Christchurch, New Zealand, 2306-2311.

Fernando, D. A. K., and Jayawardena, A. W. (1998). "Runoff forecasting using RBF networks with OLS algorithm." *Journal of Hydrologic Engineering*, 3(3), 203-209.

Garson, G. D. (1991). "Interpreting neural-network connection weights." *AI Expert*, 6(4), 46 - 51

Gaume, E., and Gosset, R. (2003). "Over-parameterisation, a major obstacle to the use of artificial neural networks in hydrology?" *Hydrology and Earth System Sciences*, 7(5), 693-706.

Hartman, E. J., Keeler, J. D., and Kowalski, J. M. (1990). "Layered neural networks with Gaussian hidden units as universal approximations." *Neural Computation*, 2(2), 210-215.

Jain, A., Sudheer, A. P., and Srinivasulu, S. (2004). "Identification of physical processes inherent in artificial neural network rainfall runoff models." *Hydrological Processes*, 18, 571-581.

Jayawardena, A. W., and Fernando, D. A. K. (1998). "Use of Radial Basis Function Type Artificial Neural Networks for Runoff Simulation." *Computer-Aided Civil and Infrastructure Engineering*, 13(2), 91-99.

Leonard, J. A., Kramer, M. A., and Unger, L. H. (1992). "Using Radial Basis Functions to Approximate a Function and Its Error Bounds." *IEEE Transactions on Neural Networks*, 3(4), 624-627.

Lozowski, A., Cholewo, T. J., and Zurada, J. M. "Crisp rule extraction from perceptron network classifiers." *IEEE International conference on neural networks: Plenary, Panel and Special sessions*, Washington DC, 94-99.

Luo, F. L., and Unbehauen, R. (1999). *Applied Neural Networks for Signal Processing*.

Park, J., and Sandberg, I. W. (1991). "Universal approximations using Radial-Basis-Function networks." *Neural Computation*, 3(2), 246-257.

Park, J., and Sandberg, I. W. (1993). "Approximation and radial basis function networks." *Neural Computation*, 5, 305-316.

Rabuñal, J. R., Dorado, J., Pazos, A., Pereira, J., and Rivero, D. (2004). "A New Approach to the Extraction of ANN Rules and to Their Generalization Capacity Through GP " *Neural Computation*, 16, 1483-1523.

Shamseldin, A. Y., Abrahart, R. J., and See, L. M. (2005). "Neural Network river discharge forecastis: An empirical investigation of hidden unit processing functions based on two different catchments." International conference on Neural Networks.

Shepherd, T. J., and Broomhead, D. S. (1990). "Nonlinear signal pocessing using radial basis functions." *SPE Advanced Signal Processing Algorithms, Architectures, and Implementations*, 1348, 51-61.

Specht, D. F. (1991). "A general regression neural network." *IEEE Transactions on Neural Networks*, 2(6), 568-576.

Sudheer, K. P., and Jain, S. K. (2003). "Radial Basis Function Neural Network for Modeling Rating Curves." *Journal of Hydrologic Engineering*, 8(3), 161-164.

Sutcliffe, J. V., and Parks, Y. P. (1999). "The hydrology of the Nile." *IAHS Special Publications*, 5, 179.

Tickle, A., Andrews, R., Golea, M., and Diederich, J. (1998). "The truth will come to light: Directions and challenges in extracting knowledge embedded within trained artificial neural network." *IEEE Transactions on Neural Networks*, 9(6), 1057-1068.

Wilby, R. L., Abrahart, R. J., and Dawson, C. W. (2003). "Detection of conceptual model rainfall-runoff processes inside an artificial neural network." *Hydrological Sciences Journal*, 48(2), 163-181.

Wu, J. S., Han, J., Annambhotla, S., and Bryant, S. (2005). "Artificial Neural Networks for Forecasting Watershed Runoff and Stream Flows." *Journal of Hydrologic Engineering*, 10(3), 216-222.

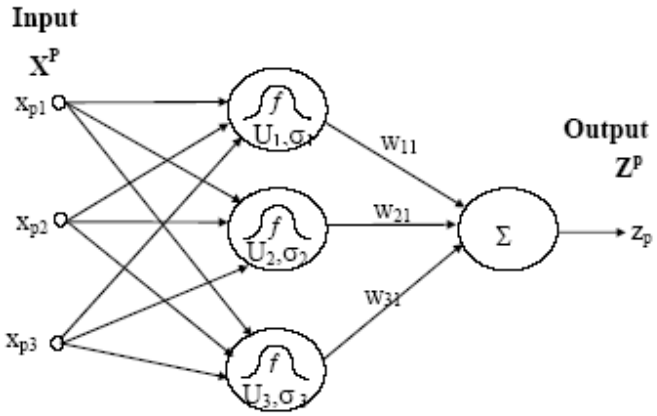


**Figure 1:** Schematic of the RBF network processing the $p^{th}$ input/output

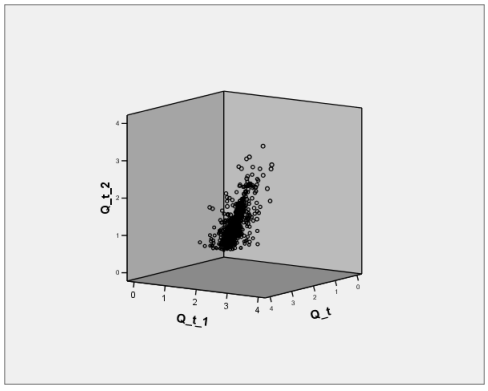


**Figure 2a:** All data points in the input space for Blue Nile River

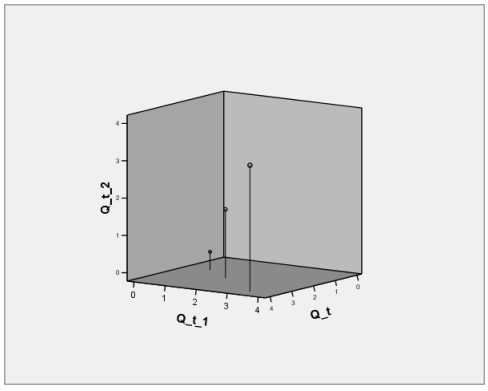


**Figure 2b:** RBF centres in the input space for Blue Nile River

[Notation: Q_t=Q(t), Q_t_1=Q(t-1),Q_t_2=Q(t-2)]

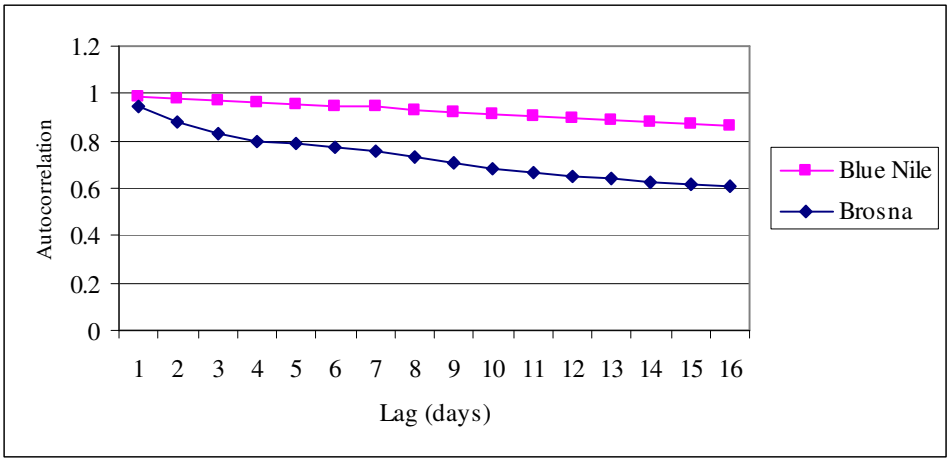


**Figure 3:** The autocorrelation of flow values for the two rivers

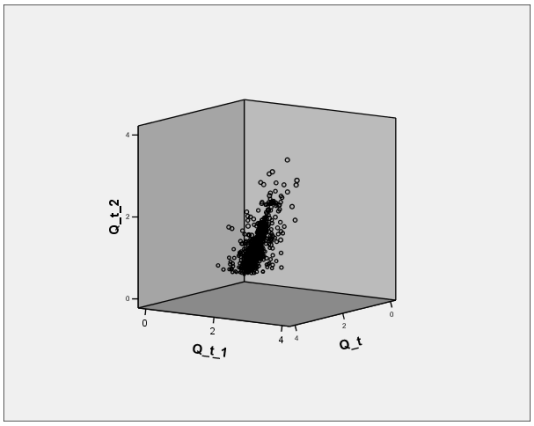


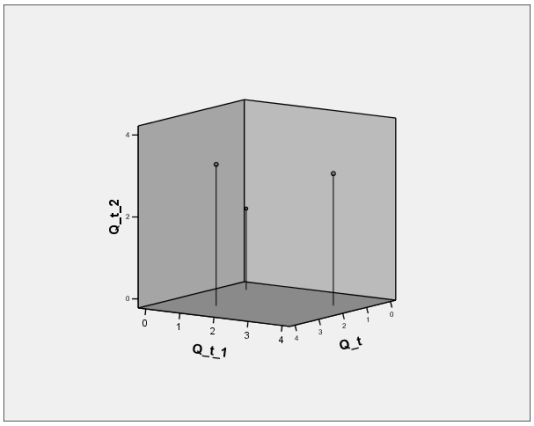


**Figure 4a:** Brosna River Input space **Figure 4b:** Brosna River RBF Locations

[Notation: Q_t = Q(t), Q_t_1 = Q(t-1), Q_t_2 = Q(t-2)]

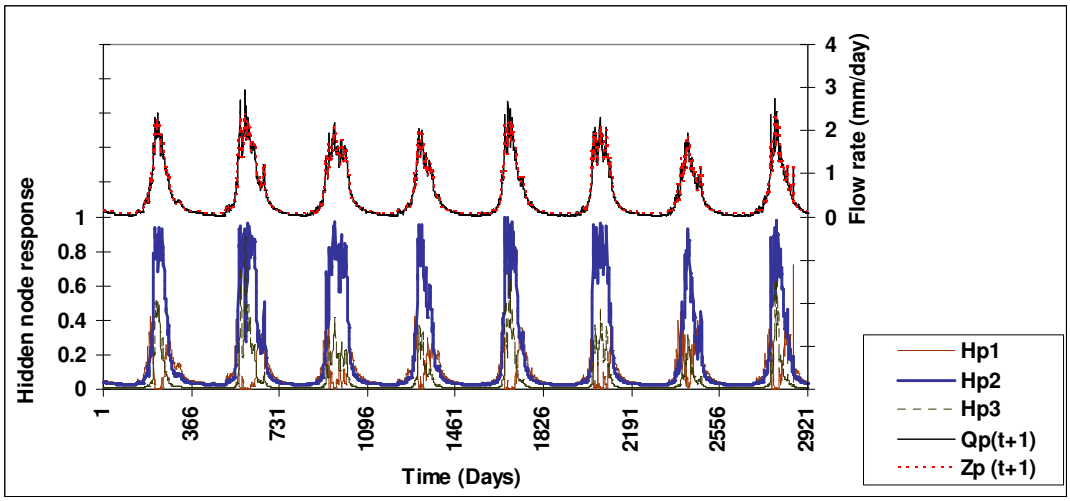


**Figure 5:** Hidden node response (Primary y-axis) and comparison of forecast and actual flows (secondary y-axis) for Blue Nile river. **$R^2$ = 96.91%**

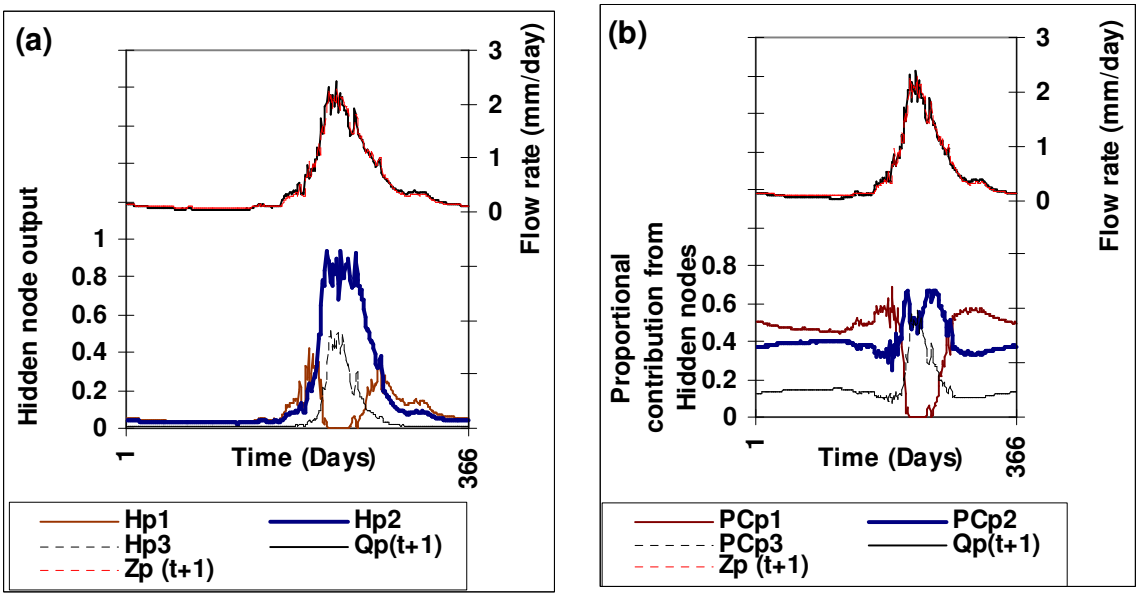


**Figure 6a:** The hidden layer response (Primary y-axis) and comparison of forecast and actual flows (secondary y-axis) for Blue Nile river for the first year **Figure 6b:** Proportion of contribution from hidden nodes (Primary y-axis) and comparison of forecast and actual flows (secondary y-axis) for Blue Nile river for the first year

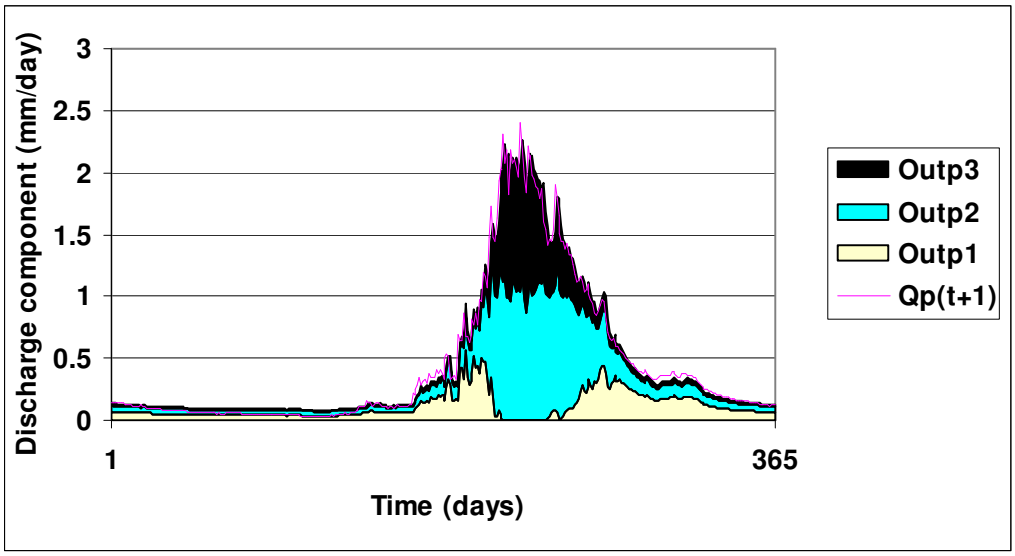


**Figure 7:** The hidden neurone contribution to output stacked up for Blue Nile river

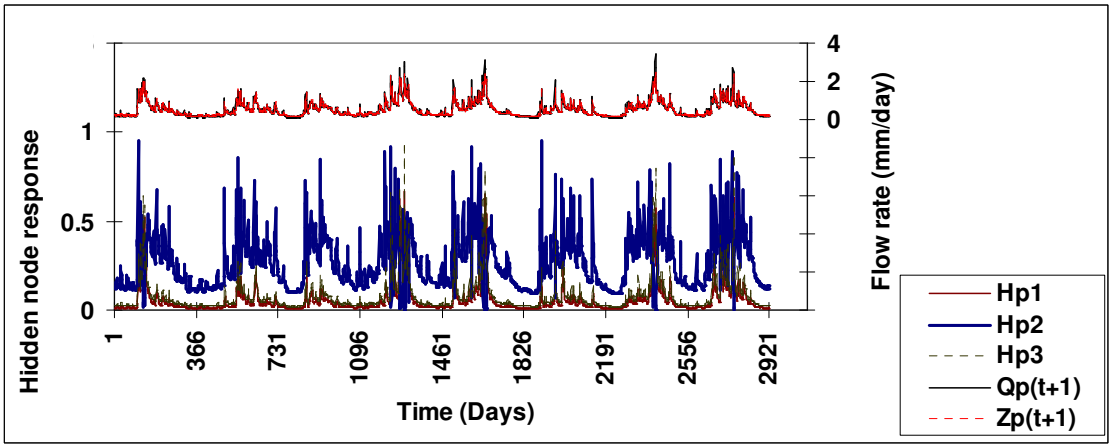


**Figure 8:** Hidden node response (primary y-axis) and comparison of forecast and actual flows (secondary y-axis) for Brosna river. **$R^2$ = 88.48%**

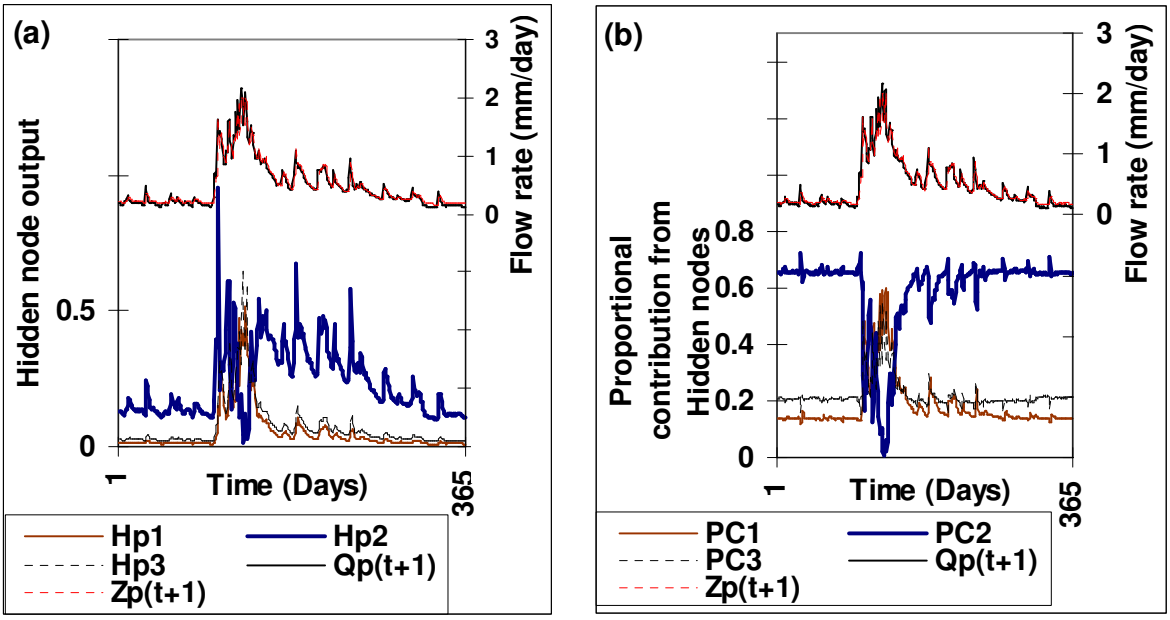


**Figure 9a:** Hidden node response (primary y-axis) and comparison of forecast and actual flows (secondary y-axis) for Brosna river for the first year **Figure 9b:** Proportional contribution from hidden nodes (primary y-axis) and comparison of forecast and actual flows (secondary y-axis) for Brosna river for the first year

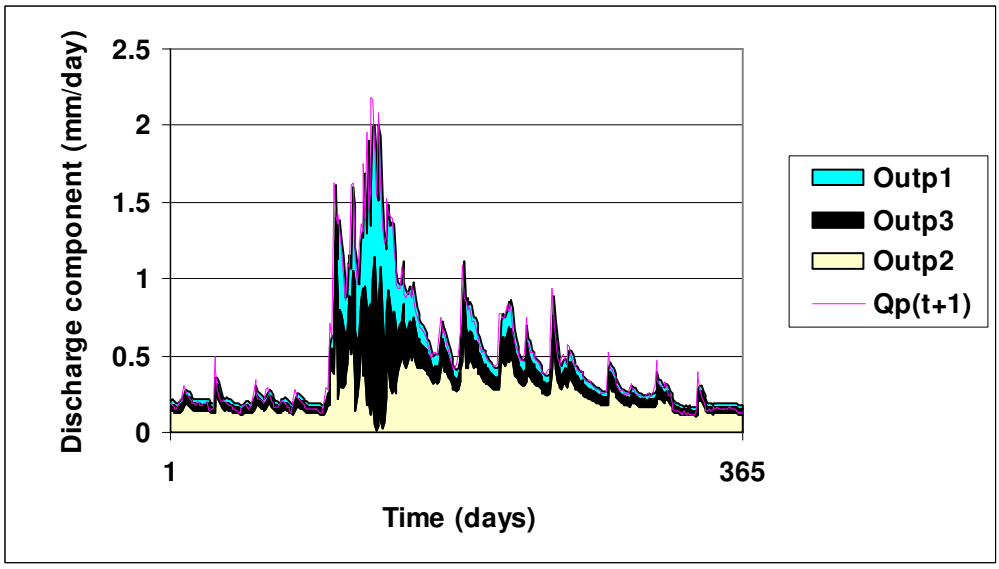


**Figure 10:** Hidden neurone contribution to output stacked up for Brosna river

**Table 1:** Summary of the data used in the study

| River | Location of flow measurement | Length of training data set (years) | Length of Testing data set (years) |
|---|---|---|---|
| Blue Nile | El Deim, Sudan | 4 | 4 |
| Brosna | Ferbane, Ireland | 4 | 4 |

**Table 2:** Flow statistics and RBF network parameters

| Catchment | Flow rate ($m^3/s$) | | | RBF Centre # | | | | Spread (sigma) | Output layer weights | | |
|---|---|---|---|---|---|---|---|---|---|---|---|
| | Min. | Max. | Mean | | Q(t-2) | Q(t-1) | Q(t) | | W1 | W2 | W3 |
| Blue Nile | 1.3 | 391.9 | 50.5 | 1 | 49.5 | 64.9 | 91.1 | 73.9 | 47.1 | 68.3 | 294.5 |
| | | | | 2 | 113.0 | 122.3 | 175.4 | 92.7 | | | |
| | | | | 3 | 258.8 | 257.2 | 336.2 | 234.8 | | | |
| Brosna | 0.1 | 3.4 | 0.5 | 1 | 2.86 | 1.11 | 3.22 | 1.98 | 2.3 | 1.0 | 1.7 |
| | | | | 2 | 0.63 | 0.43 | 1.75 | 1.16 | | | |
| | | | | 3 | 1.22 | 3.40 | 2.99 | 2.29 | | | |